



OPEN ACCESS

EDITED BY

Hock Jin Quah,
University of Science Malaysia, Malaysia

REVIEWED BY

Chih-Hsien Lai,
National Yunlin University of Science and
Technology, Taiwan
Senthilselvan Jayaraman,
University of Madras, India
Kosuke Sugawa,
Nihon University, Japan

*CORRESPONDENCE

R. Arun Prasath,
✉ raprasath.get@pondiuni.edu.in,
✉ raprasath@pondiuni.ac.in

RECEIVED 30 June 2024

ACCEPTED 24 September 2024

PUBLISHED 11 October 2024

CITATION

Joshi DN, Pal AK, Krishnapriya R and Arun
Prasath R (2024) Submicron-scale
Au-decorated TiO₂ mesoporous spheres for
enhanced photon harvesting in DSSCs
through near-field enhancement, light
scattering, and dye loading.
Front. Mater. 11:1457325.
doi: 10.3389/fmats.2024.1457325

COPYRIGHT

© 2024 Joshi, Pal, Krishnapriya and Arun
Prasath. This is an open-access article
distributed under the terms of the [Creative
Commons Attribution License \(CC BY\)](#). The
use, distribution or reproduction in other
forums is permitted, provided the original
author(s) and the copyright owner(s) are
credited and that the original publication in
this journal is cited, in accordance with
accepted academic practice. No use,
distribution or reproduction is permitted
which does not comply with these terms.

Submicron-scale Au-decorated TiO₂ mesoporous spheres for enhanced photon harvesting in DSSCs through near-field enhancement, light scattering, and dye loading

Dhavalkumar N. Joshi¹, Anil Kumar Pal², R. Krishnapriya³ and R. Arun Prasath^{1*}

¹Laboratory of Energy Materials and Suitability, Department of Green Energy Technology, Pondicherry University, Puducherry, India, ²Chair in Hybrid Nanosystems, Nanoinstitute Munich, Faculty of Physics, Ludwig-Maximilians-Universität München, München, Germany, ³Department of Chemistry, Indian Institute of Technology Jodhpur, Jodhpur, Rajasthan, India

Light harvesting materials are crucial for capturing the sunlight in a device such as a solar cell for better efficiency. In this study, we developed high surface area, submicron-sized TiO₂ spheres (MTS) incorporated with anisotropic Au nanoparticles (Au_MTS) to create highly light-absorbing photoanodes for enhanced dye-sensitized solar cell (DSSC) efficiency. The high surface area of MTS (~125 m²/g) allows for increased dye-loading, while their submicron size (150–300 nm) provides superior light-scattering capabilities for significantly enhancing the photoanode's light absorption. Furthermore, incorporating of anisotropic Au nanoparticles enables broadband surface plasmon resonance (SPR) coupling, synergistically boosting photon harvesting in the Au_MTS photoanodes. The interconnected tiny TiO₂ nanoparticle network in MTS supports charge carrier generation and transport, providing ample sites for dye adsorption and efficient electron pathways. Au_MTS with varying amounts of Au nanoparticles synthesized by a greener microwave-assisted synthesis method and DSSC devices were fabricated and compared with devices made from pristine MTS and P25 nanoparticles. The optimal Au_MTS device, containing ~1.3 wt% Au nanoparticles, achieved a maximum power conversion efficiency (PCE) of ~7.7%, representing improvements of ~40% and ~60% over pristine MTS (PCE of ~5.2%) and P25 nanoparticles (PCE of ~4.71%), respectively. Overall, this work demonstrates the effectiveness of plasmonic mesoporous photoanodes in enhancing DSSC performance through improved photo response, light scattering, and dye loading.

KEYWORDS

mesoporous structures, dye-sensitized solar cell, surface plasmon resonance, light-scattering, electron transport

1 Introduction

The demand for renewable energy is determinedly increasing to fulfill the energy demand without impairing the environment. In this scenario, third-generation solar cells have attracted broad attention to generating electricity with low-cost, non-toxic materials to promote sustainable and environmentally friendly technology. Among the 3rd generation solar cells, the dye-sensitized solar cells (DSSCs), the predecessor of currently developed perovskite solar cell technologies (PSCs), still have significant scope for performance and stability improvement and attracted substantial interest in the scientific community due to their simple fabrication method, economical energy payback time and especially their ability to work under the diffuse light environment (O'regan and Grätzel, 1991; Gonçalves et al., 2008; Gonçalves et al., 2009; Hagfeldt et al., 2010; Jung and Lee, 2013). The morphology of the photoanode, determining the light-harvesting and charge carrier transport, significantly affects the device's efficiency. Conventionally, TiO₂ nanoparticles with an average size of ~25 nm (P25) have been used in the fabrication of photoanode films in DSSCs. The high number of grain boundaries and recombination sites in mesoporous structures deteriorates the device performance in P25 based nanostructure. The application of nanotubes and nanorods to improve the charge transport limits the efficiency due to poor dye-loading, impacted by the inferior surface area of these structures. Further, conventional P25 NPs photoanode film possesses poor light absorption due to negligible light scattering, leading to loss of large wavelength photons and subsequently limits the PCE. The additional light scattering layer of sub-micron size TiO₂ NPs is applied on top of the active TiO₂ layer (Joshi et al., 2017). However, efficiency enhancement is limited due to the poor electrolyte diffusion and the charge carrier recombination. Hence, it is necessary to improve the light absorption by scattering effects while maintaining a high internal surface area of the photoanode films for efficient dye adsorption and electrolyte diffusion. The efforts have been implemented to modify the photoanode structure, such as utilizing hierarchical nanostructures to enhance the device efficiency by controlling the light absorption, electron transport, and reducing interfacial recombination (Wang et al., 2013; Krishnapriya et al., 2015; Lim et al., 2015; Mohammadian-Sarcheshmeh et al., 2020; Choudhury et al., 2021).

A significant improvement in the light-harvesting of the photoanode has been reported by applying the mesoporous sub-micron size TiO₂ sphere, enhancing optical path length in the photoanode via light scattering (Yang et al., 2010; Dong et al., 2014; Ding et al., 2015; Li et al., 2015; Dissanayake et al., 2020). Further, the application of the localized surface plasmon resonance (LSPR) from the noble plasmonic NPs has also shown remarkable achievement in the PCE enhancement by improving the light absorption by the dye molecules (Atwater and Polman, 2010; Jang et al., 2016; Mandal and Sharma, 2016; Sharifi et al., 2016; Tran et al., 2016; Zarick et al., 2016; Moradi et al., 2020; Kaur et al., 2022; Vemula and Raavi, 2022; Li et al., 2023).

Herein, microwave-synthesized Au_MTS spheres were utilized to synergize the light scattering and SPR coupling to improve light harvesting in the DSSCs. The Au_MTS sub-micron structures offer several advantages: (1) Enhanced dye adsorption capacity in the photoanode due to the high surface area of MTS, (2) Improved light

absorption through broadband localized surface plasmon resonance (LSPR) from anisotropic AuNPs, enhancing dye-mediated photon capture, (3) Enhanced light scattering at longer wavelengths by sub-micron-sized TiO₂ spheres, effectively lengthening the optical path within the photoanode, and (4) Facilitated smooth electron transport enabled by the well-connected network of Au-MTS composite nanostructures. Thus, the synergistic light scattering, dye loading, and plasmonic enhancement boost the light-harvesting ability and improve the performance of the devices substantially. The designed Au-MTS fabricated DSSCs device showed a phenomenal improvement in the PCE of ~60% compared to reference devices fabricated with P25 TiO₂ NPs.

2 Results and discussion

Au_MTS with varying AuNP loadings was synthesized by incorporating irregular shape and sizes of Au nanoparticles (Mx-AuNPs), prepared via a DMF-based microwave-assisted chemical reduction method (Joshi et al., 2022). The AuNPs were introduced into titanium glycolate precursor solutions at different weight percentages, ranging from 0.25 wt% to 2 wt%, during the synthesis process. The resulting materials were designated as Au_MTS-X (X = 1,2,3,4 denotes the wt% of Mx-AuNPs in MTS 0.25, 0.5, 1 and 2, respectively). Figure 1A depicts the UV-Vis diffuse reflectance spectra (DRS) of P25, as-synthesized MTS, and Au_MTS samples with varying Au loadings. The broad absorption feature centered around 550 nm, present in the spectra of Au_MTS but absent in P25 and MTS, is indicative of the broadband surface plasmon resonance (SPR) associated with the Mx-AuNPs. As the Au loading in MTS increases from 0.25 wt% to 2 wt%, a progressive enhancement in the intensity of the SPR band is observed, accompanied by a red-shift toward longer wavelengths. This shift is attributed to the increasing aggregation of Mx-AuNPs with higher loading percentages.

Figures 1B, C display the XRD spectra of pristine MTS samples, compared with standard P25 NPs and Au_MTS samples, respectively. In pristine MTS samples, all diffraction peaks can be indexed to a pure anatase phase structure (JCPDS Card No. 21-1272). No peaks related to the rutile structure are observed, unlike in P25 NPs, confirming the phase purity of the MTS samples (JCPDS Card No: 21-1276).

The significantly broadened diffraction peaks indicate the formation of nanocrystalline MTS samples. Based on the Scherrer equation, the crystallite size of the pristine MTS samples is estimated to be approximately 7.5 nm, calculated from the FWHM of the primary (101) peak. This crystalline anatase structure, with small crystallites, is suitable for dye loading and efficient electron transport in DSSC applications. In Au_MTS-X (X = 1,2,3,4) samples, especially at high Au-loading, a tiny 2θ peak appears around 44.3°, which can be assigned to the (200) planes of the Au NPs. Another diffraction peak from the AuNPs around 38.1° corresponding to the (111) might have merged with the diffraction peaks from the anatase phase of MTS.

Figure 2 shows high-resolution SEM (HRSEM) images of MTS and Au_MTS-3 (the best-performing sample). The images reveal the presence of large, porous, flocky spheres ranging from 150 to 250 nm, with tiny TiO₂ nanoparticles uniformly adhered to one another. The magnified images of the TiO₂ spheres,

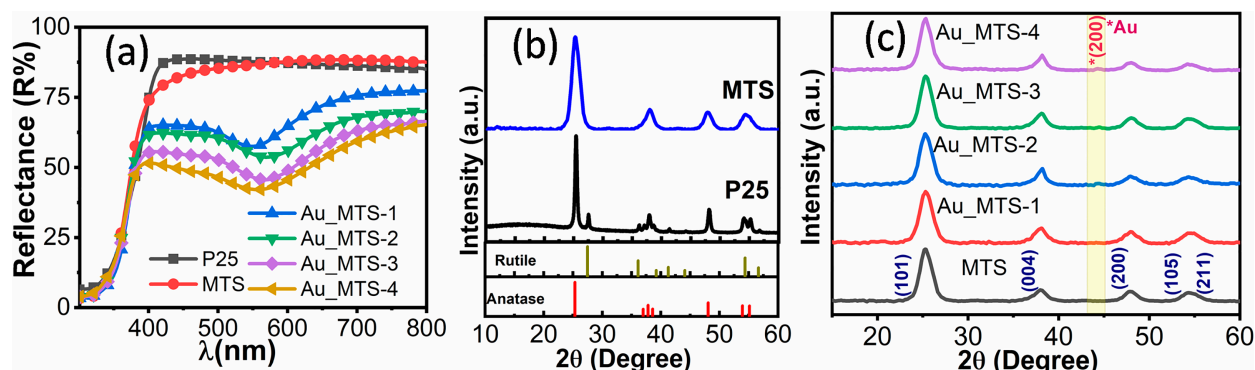


FIGURE 1 UV-Vis DRS and XRD spectra of the different powder samples, (A) UV-Vis spectra, (B) XRD spectra of pristine MTS and P25 NPs, and (C) XRD Spectra of the Pristine MTS and different Au_MTS samples.

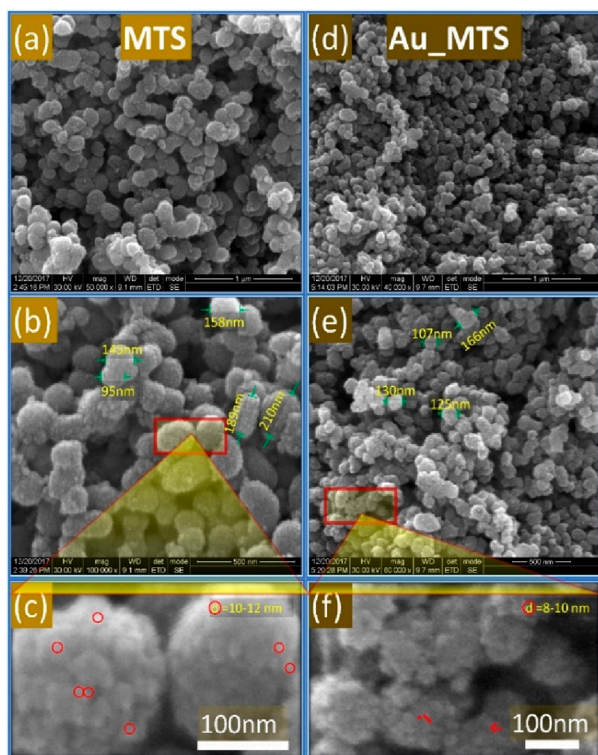


FIGURE 2 HRTEM image at different magnifications of the MTS at (A) 50K, (B) 100K, and (C) enlarged and Au_MTS samples (D) 50K, (E) 100K, and (F) enlarged.

highlighted with red circles in Figures 2C, F, show that each sphere is composed of interconnected nanoparticles, approximately 9 nm in size. This arrangement offers a substantial surface area, making the MTS structures highly suitable for loading significant amounts of light sensitizer dye. The surface areas of the MTS and Au_MTS samples were measured at approximately 125 m²/g and 115 m²/g, respectively, surpassing that of standard P25 nanoparticles (60 m²/g). The high surface area, despite the larger submicron-sized spheres, is a unique characteristic of the MTS structures.

The submicron size range of 150–250 nm is comparable to the wavelength of visible light, promoting efficient light scattering within the photoanode. This increases the optical path length, thereby enhancing the probability of photon absorption in the device. The particle size of the TiO₂ spheres slightly decreases in the Au_MTS samples, as shown in Figures 2B, E. This reduction is likely due to the addition of AuNPs dispersed in ethanol during the synthesis process, which results in a minor alteration of the reaction solvent composition.

Figure 3 shows the TEM images of the MTS and Au_MTS-3 samples. The images clearly reveal the packed and closely interconnected nanocrystals with sizes around 7–8 nm in the MTS structures. This observed crystallite size coincides with the calculated crystallite size from the XRD spectra. Such interconnected structures suggest good charge transport properties of the material. Lattice fringes can be observed in the HRTEM image of Au_MTS in Figure 4A, indicating the crystalline nature of the materials. The observed lattice spacing of approximately 0.35 nm can be attributed to the (101) planes of the anatase phase. The concentric circular selected area electron diffraction (SAED) pattern of bright spots observed in Figure 4B indicates the polycrystalline nature of the MTS. The concentric circular SAED pattern of bright dots suggests the polycrystalline nature of the MTS (Figure 4B).

The cumulative data from XRD, FESEM, BET, and TEM analyses suggest that the as-synthesized MTS possesses good crystallinity, sub-micron size, high surface area, and an interconnected network. These properties indicate superior light absorption and efficient electron transport in the materials, which are essential for fabricating high-efficiency devices. The as-synthesized MTS, Au-MTS-1, Au-MTS-2, Au-MTS-3, Au-MTS-4, and commercial P25 nanoparticles were deposited on the FTO glass substrate using the doctor blading method, followed by annealing at 500°C. The UV-Visible-DRS absorption spectra of the films and the respective photoanodes are shown in Figures 5A, B. In Figure 5A, the observed broad absorbance peak in the 500–700 nm region is attributed to the SPR effect of the AuNPs, which is absent in pristine MTS and P25 nanoparticles. Notably, there is a redshift in the SPR peak with increasing AuNPs loading (wt%) in MTS, likely due to the aggregation of AuNPs. As the loading amount increases, the AuNPs

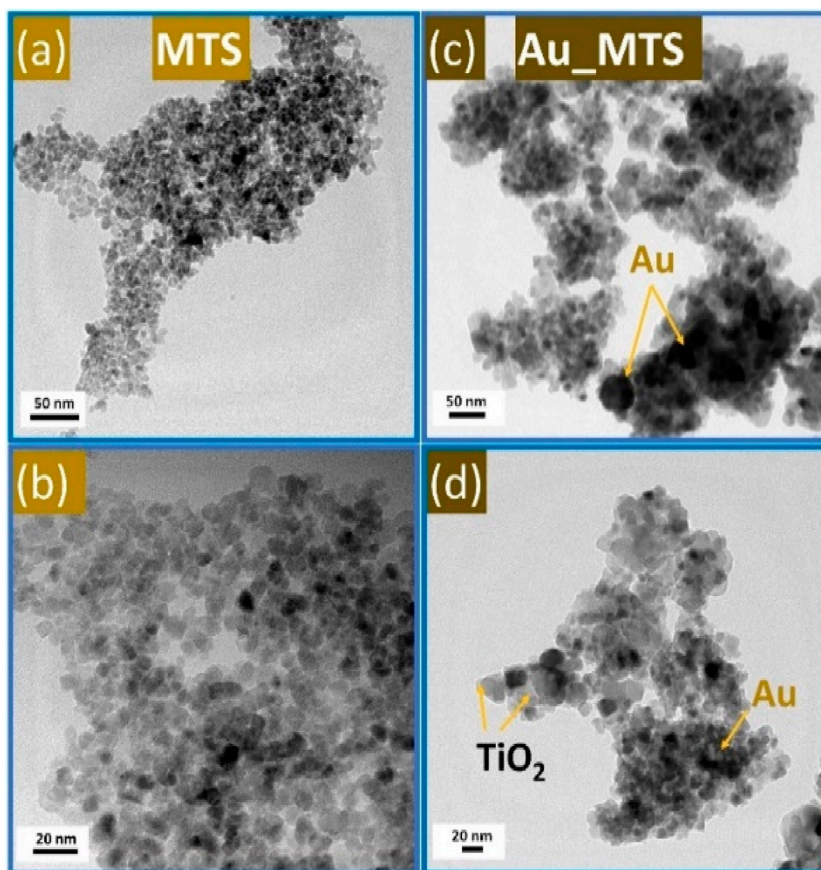


FIGURE 3 TEM images of (A, B) MTS and (C, D) Au_MTS samples at different magnifications.

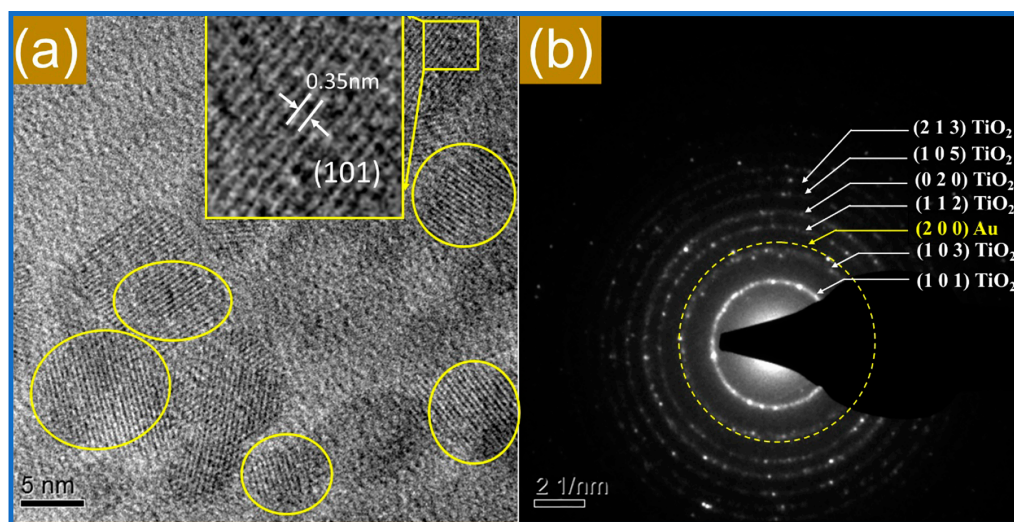


FIGURE 4 (A) Lattice fringes and (B) SAED pattern of the Au_MTS sample.

density in the MTS matrix rises, promoting aggregation during annealing and resulting in a redshift in SPR. A similar SPR-induced improvement in absorbance is observed in the dye-loaded MTS film when incorporated with AuNPs, with the Au-MTS-4

photoanode showing the highest absorbance peak around 550 nm. The absorbance peaks become slightly broader and red-shifted for the Au-MTS photoanode films compared to pristine MTS and P25 films due to the overlapping peak maxima of the dye and

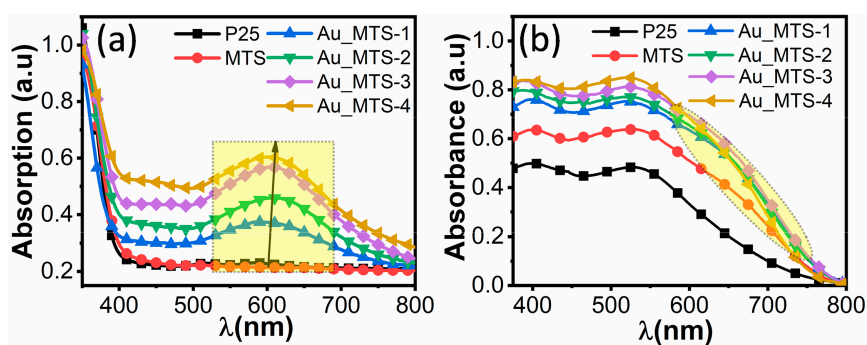


FIGURE 5 UV-Visible Diffuse Reflectance Spectra (UV-VIS-DRS) of P25, MTS and Au incorporated MTS (A) Fabricated TiO_2 Film (B) Photoanode (TiO_2 -Dye) film.

TABLE 1 Average light absorbance of the photoanode film in different wavelength region.

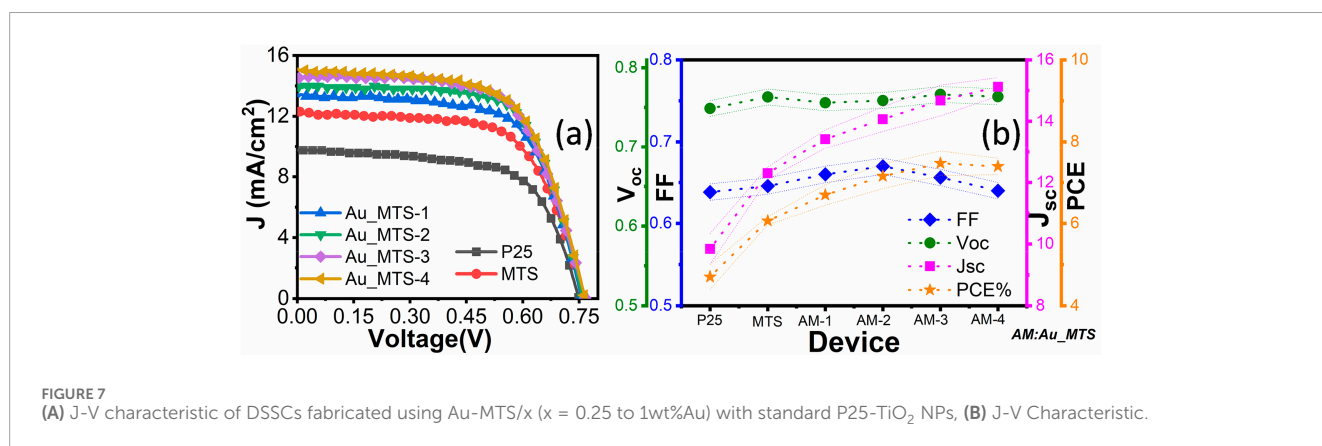
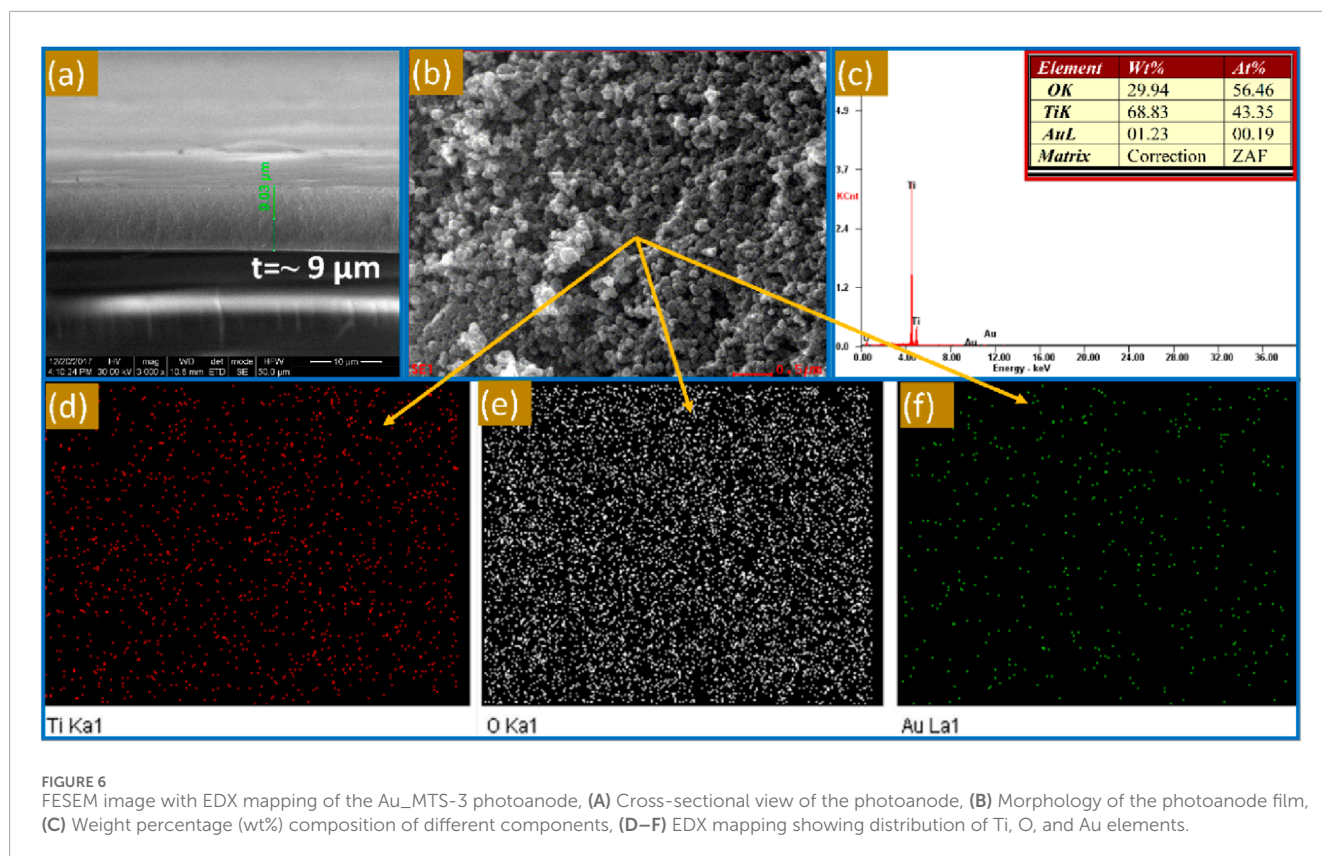
Average absorbance (%)	P25	MTS	AM-1	AM-2	AM-3	AM-4	ΔA_{avg} (P25/AM-3)	ΔA_{avg} (MTS/AM-3)
(a) Dye-Active 450–600 nm	39.9	60.5	71.5	74.0	77.6	80.5	↑ 37.7	↑ 17.1
(b) SPR-Active 550–700 nm	29.2	56.8	68.0	70.3	74.2	75.5	↑ 45.0	↑ 17.4
(c) MTS-active 600–750 nm	9.2	31.3	41.3	41.3	44.4	39.4	↑ 35.2	↑ 13.1
Total 400–800 nm	24.1	42.2	52.1	53.4	56.4	55.5	↑ 32.3	↑ 14.2

* AM, Au_MTS.

SPR of the AuNPs. The significantly higher surface area of MTS ($\sim 125 \text{ m}^2/\text{g}$ compared to $\sim 60 \text{ m}^2/\text{g}$ for P25 NPs) enhances their dye-loading capability, resulting in considerably higher absorbance for the MTS photoanode compared to P25. Importantly, MTS photoanodes (Figure 5B) show a clear improvement in absorbance in the longer wavelength region (i.e., 600–700 nm) compared to the P25 photoanode, attributed to photon scattering from the larger MTS particles. According to the Rayleigh scattering phenomenon, when particle size is comparable to a particular wavelength, they tend to scatter light, enhancing the optical path length and light absorption capacity of the film. This photon scattering phenomenon, present in MTS-based photoanode films, is absent in the P25 photoanode film. The calculated average absorbance and enhancement in the absorbance of the photoanode films are presented in Table 1. In the (a) dye-active (450–600 nm), (b) SPR-active (550–700 nm), and (c) MTS-active (600–700 nm) regions, light absorbance is primarily due to the amount of dye loaded on the TiO_2 film matrix (a), SPR from the AuNPs (b), and photon scattering from larger TiO_2 particles (c), respectively. Thus, it is clear that with synergistic effects of high surface area, large particle size, and AuNPs loading, the MTS and Au-MTS photoanodes exhibit significantly improved light absorbance in all three regions (a-c). The best-performing Au-MTS-3 photoanode film enhances total light harvesting by 32.3% compared to commercial P25% and 14.2% compared to pristine MTS. Notably, despite the higher surface area of MTS-based photoanodes, which would typically result in better dye loading and enhanced light

absorption, the light absorption in Au_MTS-based photoanodes surpasses that of MTS-based photoanodes. This enhanced light absorption in Au_MTS-based photoanodes is primarily attributed to the localized surface plasmon resonance (LSPR) effect of the Mx-AuNPs. Secondly, as evident from the Figure 1A, the matching of LSPR energy to the optical absorption energy of MTS facilitated the plasmon resonance energy transfer (PRET) from Au nanoparticles to MTS molecules and the resonance coupling of LSPR to molecular dipole of dye molecules promote the fluorescence enhancement. On top of that, the electron transfer may occur from Au nanoparticles to the dye molecule as a result of physical contact between them, enabling further light enhancement. The near-field enhancement and far-field scattering effects of these nanoparticles improve the light absorption by the dye molecules in their vicinity and extend the optical path length within the photoanode, respectively, leading to overall improved light absorption.

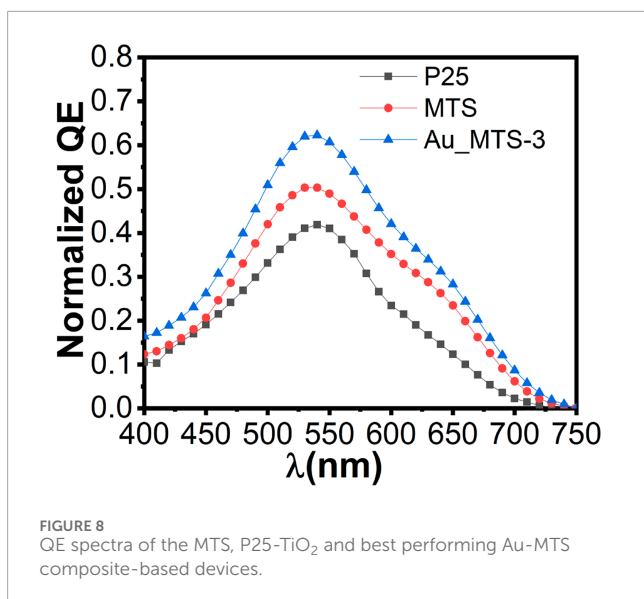
Figure 6A shows the cross-sectional view of the photoanode film fabricated using Au_MTS-3 with the doctor blading method. The film thickness is approximately $9 \mu\text{m}$, and it adheres well to the FTO substrate. The morphology of the Au_MTS spheres (Figure 6B) clearly shows large microspheres (150–200 nm) interconnected with high porosity, which is desirable for high dye loading. Further EDX mapping (Figures 6D–F) demonstrates the uniform dispersion of Au nanoparticles within the photoanode, with an approximate loading of 1.23 wt% (Figure 6C). This dispersion of AuNPs is beneficial for synergistic light absorption, enhancing light capture in the



vicinity of the dye molecules due to the plasmonic effect of the Au nanoparticles.

As discussed in the device fabrication section, the devices were fabricated by sandwiching the photoanode and Pt-based cathode. Figure 7A shows the J-V curves of the DSSCs fabricated using MTS, P25-TiO₂, and various Au-MTS-X (x = wt% Au = 0, 0.25, 0.5, 1.00, and 2.00) composites. The characteristic open-circuit voltage (V_{oc}), short-circuit current density (J_{sc}), fill factor (FF), and photoconversion efficiency (PCE) data are compared in Figure 7B. The results reveal that increasing the loading of AuNPs in MTS has substantially changed the PCE, primarily driven by an increase in J_{sc}, with minor changes in FF and V_{oc}. The constant V_{oc} value indicates that the TiO₂ Fermi level does not change significantly

with the presence of AuNPs, as the potential difference between the TiO₂ Fermi level and the redox potential of the electrolyte primarily determines V_{oc}. The devices based on P25 NPs showed lower J_{sc} and PCE compared to those based on MTS. The J_{sc} of MTS-based DSSCs increased to 11.19 mA/cm², compared to 9.84 mA/cm² for P25-TiO₂-based DSSCs. Consequently, the PCE of the MTS-based device improved to 5.51%, a 16% enhancement compared to the P25-TiO₂-based DSSC device (PCE = 4.71%). The J-V data demonstrate that increased J_{sc} values primarily drive the observed enhancement. This improvement in MTS-based DSSCs can be attributed to enhanced charge carrier generation facilitated by superior light absorption capacity. The larger spherical size of MTS (Figure 2) contributes to effective light scattering, while their high surface



area enables greater dye loading in the photoanode (Figure 5). These factors establish a clear correlation between the observed enhancement in J_{sc} values and the mechanisms underlying improved charge carrier generation in MTS-based DSSCs, emphasizing the importance of light absorption capacity and surface area for efficient dye loading. Additionally, DSSCs fabricated with Au_MTS-1 to Au_MTS-4 exhibited increased J_{sc} values to 13.03, 13.89, 14.34, and 14.96 mA/cm², respectively, with minor changes in FF and V_{oc} . The data demonstrate a gradual increase in J_{sc} with higher concentrations of AuNPs in MTS. Notably, DSSCs fabricated using MTS with ~1% wt. of AuNPs (Au-MTS-3) achieved a PCE of approximately ~7.7%, marking a significant improvement of ~40% compared to MTS-based DSSCs (PCE ~5.51%) and ~60% compared to P25-TiO₂-based DSSCs (PCE ~4.71%). These results clearly illustrate that incorporating AuNPs into MTS substantially enhances both J_{sc} and PCE in DSSCs. The progressive increase in J_{sc} followed by PCE suggests that incorporating AuNPs into MTS significantly enhances the photoanode's absorption capacity, enabling adjacent dyes to absorb photons (see Figure 5) effectively. These findings indicate that the synergistic effect of improved absorbance in Au-MTS composite-based photoanodes effectively enhances photo-charge carrier generation in DSSCs, thereby boosting overall PCE. In MTS-based DSSCs, the enhancement in PCE (~25%) is primarily attributed to light scattering from the spheres. Conversely, in Au-MTS composites, the synergistic effect of radiative plasmonic resonance processes from anisotropic AuNPs and light scattering from the spheres significantly enhances light-harvesting, resulting in a PCE increase of up to ~60% compared to blank DSSC devices.

To further investigate the light-harvesting capability of Au-MTS-based DSSCs, we characterized the best-performing plasmonic device using QE spectroscopy and compared it with the photo-response of MTS and P25-TiO₂-based DSSCs (Figure 8). The QE spectra show increased intensity across the entire visible spectrum for both MTS and Au_MTS composites compared to P25-TiO₂-based DSSCs (see Figure 2). This enhancement trend correlates with J_{sc} , indicating improved light-harvesting and photo-response in devices fabricated with MTS and Au_MTS

composites. Although MTS has a higher surface area than Au_MTS, which would generally result in greater dye loading and enhanced light absorption, leading to increased short-circuit current (J_{sc}) and quantum efficiency (QE), Au_MTS-based DSSCs still outperform their MTS counterparts. This superior performance is primarily due to the surface plasmon resonance (SPR) effect of the AuNPs, which boosts light absorption by the dye molecules via near-field scattering. Moreover, the far-field scattering effect from the larger AuNPs further extends the optical path in Au_MTS-based DSSCs, contributing to the overall enhancement in J_{sc} and QE. A notable enhancement is observed in the longer wavelength region (600–750 nm) for MTS- and Au_MTS-based DSSCs, which follows a similar trend seen in the UV-Vis absorption spectra of photoanodes fabricated with MTS and Au_MTS composites (Figure 5). This enhancement confirms the contribution of light scattering from the TiO₂ spheres, as well as surface plasmon resonance (SPR)-mediated light coupling between the Mx-AuNPs, particularly in the longer wavelength region.

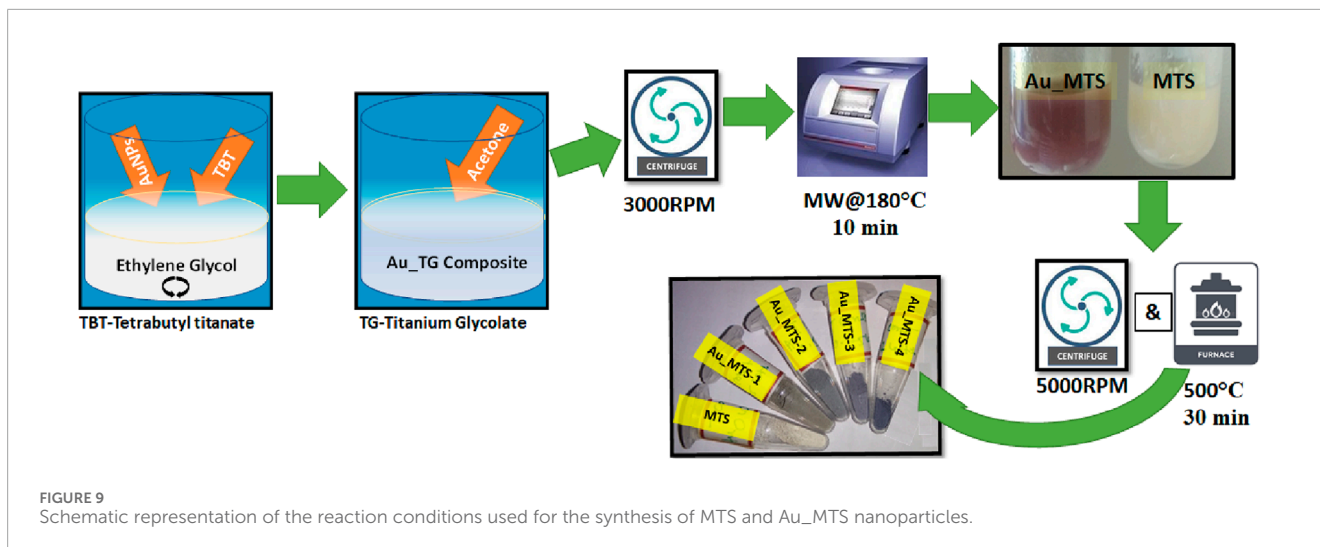
3 Conclusion

AuNPs incorporated mesoporous TiO₂ sphere (Au-MTS) were synthesized via the greener microwave-assisted hydrothermal method. The MTS and Au-MTS fabricated photoanode films showed improved light-harvesting ability compared to commercial P25-TiO₂ based photoanode due to the plasmonic effect of AuNPs, and Rayleigh scattering from MTS. In addition, Au-MTS nanocomposite-based DSSC devices were found to facilitate smooth charge transport and improved dye-loading due to their well-connected interlinked mesoporous structure. The maximum PCE of ~7.7% was achieved for the DSSC device fabricated with Au-MTS/1 (~1 wt% AuNPs loaded MTS). The observed improvement in the PCE is ~40% and ~60% higher compared to MTS-DSSCs and P25-TiO₂-DSSCs, respectively. This work revealed that the Au-MTS nanocomposite with a porous network structure combined with the plasmonic AuNPs could be utilised for better light harvesting as a photoactive material to improve the light-harvesting ability in photovoltaic and photocatalytic systems.

4 Experimental section

4.1 Materials and methods

TiCl₄ (99%)- Spectrochem was diluted in deionized water (DI) to prepare a 40 mM aqueous solution for use. Titanium (IV) butoxide-TBT (97%) (Sigma-Aldrich), ethylene glycol-EG (99.8%) (Merck), Auric chloride -HAuCl₄-(Sigma-Aldrich), Polyvinyl pyrrolidone-PVP-40,000M.W (Sigma Aldrich), fluorine doped tin oxide coated transparent (FTO) glass (8 Ω/Sq)- Sigma Aldrich, acetone (98%), ethanol (99.5%) were purchased and used as received. The materials such as Ru N719 dye, redox electrolyte (EL-HPE) and Pt-paste, Surlyn Sealant were purchased from Dyesol to fabricate the DSSCs. TiCl₄ (99%)- Spectrochem was diluted in deionized water (DI) to prepare a 40 mM aqueous solution for use.



4.2 Synthesis of the TiO₂ and TiO₂-Au sphere

To attain the broadband photon harvesting two types of nanoparticles were synthesized 1.) Mixed shapes of AuNPs (Mx-AuNPs-for broadband SPR coupled harvesting) 2) High surface area mesoporous TiO₂ sphere (MTS-for improved harvesting by high light-sensitizer loading and light-scattering). The mixed shape of AuNPs (Mx-AuNPs) were synthesized by chemical reduction of 50 mM Au salt in mixture of 10 mM PVP in DMF.

The synthesis of the TiO₂ sphere (MTS) was carried out as per the literature with slight modifications (Wang et al., 2011). In detail, the titanium glycolate precursor was synthesized by dissolving 1 mL of TBT in the 40 mL of ethylene glycol (EG). Upon addition of the TBT in, EG, the white translucent formed subsequently transforms into a transparent solution. The as-prepared mixture was quickly added to the acetone bath, which contained 150 mL of acetone with a trace amount of water. The white precipitate that forms immediately reveals the formation of the titanium glycolate. The as-formed mixture was stirred for 20 min and allowed to settle for 1 h aging. The resulting white precipitate (titanium glycolate) was collected and dried at 60°C for 24 h. To synthesising the porous TiO₂ sphere, the collected precipitate (~0.5 g) was dispersed in the mixture of 20 mL of water and ethanol (1:1) in the 30 mL microwave vessel and loaded into the microwave reactor for heating at 180°C for 15 min. The as-prepared sample was collected using centrifugation and washed several times using water and finally with ethanol to remove any impurities and unreacted, EG before drying at 60°C for 24 h. The resultant sample was heated at 500°C for 30 min to obtain the TiO₂ sphere.

To synthesize TiO₂-Au composites (Au_MTS-x, x = 1,2,3,4), Mx-AuNPs were first prepared according to the method described in our earlier publication (Joshi et al., 2022). Specifically, Mx-AuNPs were obtained by reducing 1 mL of 50 mM HAuCl₄ with 5 mM polyvinylpyrrolidone (PVP), which served as both a stabilising and reducing agent, in 15 mL of N,N-dimethylformamide (DMF), acting as the solvent and mild reducing agent. The reaction mixture was subjected to microwave irradiation at a controlled temperature of 160°C for 3 min, resulting in the formation of irregularly shaped

AuNPs (Mx-AuNPs). The as-synthesized Mx-AuNPs were centrifuged for careful solvent exchange to ethanol. The highly concentrated ~10 mg/ml Mx-AuNPs dispersion was made and used for the further reaction. Varying amounts of the as-prepared Mx-AuNPs were added to the mixture of tetrabutyl titanate (TBT) and ethylene glycol (EG) prior to the aceto-precipitation step. The subsequent synthesis of Au_MTS composite spheres followed the same procedure used for the preparation of MTS. The schematic representation of the synthesis process for MTS and Au_MTS is illustrated in Figure 9.

4.3 Fabrication of DSSCs

The Au-MTS composite spheres were deposited on TiCl₄-treated (40 mM, 70 °C) FTO glass substrate by doctor blade technique using 3-M Scotch tape as a masking layer with a thickness of ~15 μm. The as-prepared film was annealed at 500 °C for 30 min at a heating rate of 3°C/min in a furnace. Once the annealed film cooled down to 80°C, the films were immersed in 0.5 M N719 dye solution (prepared using a 1:1 mixture of acetonitrile and butanol) for 18 h for dye uptake. After the sensitization, the as-prepared photoanodes were cleaned using 2-propanol to remove the excess dye molecules from the substrate. The Pt counter electrodes were fabricated by coating Pt-paste on FTO glass substrate followed by annealing at 450 °C for 30 min. The photoanode and counter electrode were sandwiched together by Surlyn film with a thickness of ~25 μm as a spacer using binder clips. The high-performance electrolyte was introduced into the inter-electrode gap of a sandwiched device. For comparison purposes, the film with P25-TiO₂ NPs and as-synthesised TiO₂ were also prepared. A minimum of five numbers of the fabricated DSSCs for each material composition was prepared and studied for their performance.

4.4 Characterization techniques

The absorbance spectra of as-synthesized TiO₂, Au-MTS, and the active photoanodes were measured using

UV-Visible-NIR with a Keithley 2,400 current source meter and by using a 300 W Xenon source as a light source. The solar simulator with 1 Sun illumination, i.e. 100 mW/cm² was obtained using an AAA class solar simulator fixed with a 1.5 a.m. filter within the area of 2 × 2 cm. The Quantum efficiency (QE) was measured using Bentham PVE300-Quantum efficiency measurement system without bias light.

Data availability statement

The original contributions presented in the study are included in the article/supplementary material, further inquiries can be directed to the corresponding author.

Author contributions

DJ: Conceptualization, Data curation, Formal Analysis, Investigation, Methodology, Resources, Validation, Visualization, Writing—original draft, Writing—review and editing. AP: Formal Analysis, Writing—review and editing. RK: Data curation, Writing—review and editing. RA: Funding acquisition, Project administration, Supervision, Writing—review and editing.

References

- Atwater, H. A., and Polman, A. (2010). Plasmonics for improved photovoltaic devices. *Nat. Mater.* 9, 205–213. doi:10.1038/nmat2629
- Choudhury, B. D., Lin, C., Shawon, S. M. A. Z., Soliz-Martinez, J., Huq, H., and Uddin, M. J. (2021). A photoanode with hierarchical nanoforest TiO₂ structure and silver plasmonic nanoparticles for flexible dye sensitized solar cell. *Sci. Rep.* 11, 7552. doi:10.1038/s41598-021-87123-z
- Ding, Y., Zhou, L., Mo, L., Jiang, L., Hu, L., Li, Z., et al. (2015). TiO₂ microspheres with controllable surface area and porosity for enhanced light harvesting and electrolyte diffusion in dye-sensitized solar cells. *Adv. Funct. Mater.* 25, 5946–5953. doi:10.1002/adfm.201502224
- Dissanayake, M., Senthuran, S., and Senadeera, G. K. R. (2020). Efficiency enhancement in dye-sensitized solar cells using hierarchical TiO₂ 2 submicron size spheres as a light scattering layer. *J. Solid State Electrochem.* 24, 2261–2269. doi:10.1007/s10008-020-04727-7
- Dong, Z., Ren, H., Hessel, C. M., Wang, J., Yu, R., Jin, Q., et al. (2014). Quintuple-shelled SnO₂ hollow microspheres with superior light scattering for high-performance dye-sensitized solar cells. *Adv. Mater.* 26, 905–909. doi:10.1002/adma.201304010
- Gonçalves, L. M., de Zea Bermudez, V., Ribeiro, H. A., and Mendes, A. M. (2008). Dye-sensitized solar cells: a safe bet for the future. *Energy Environ. Sci.* 1, 655–667. doi:10.1039/b807236a
- Gonçalves, L. M., de Zea Bermudez, V., Ribeiro, H. A., and Mendes, A. M. (2009). Dye-sensitized solar cells: a safe bet for the future. *Energy Environ. Sci.* 1, 655. doi:10.1039/b807236a
- Hagfeldt, A., Boschloo, G., Sun, L., Kloo, L., and Pettersson, H. (2010). Dye-sensitized solar cells. *Chem. Rev.* 110, 6595–6663. doi:10.1021/cr900356p
- Jang, Y. H., Jang, Y. J., Kim, S., Quan, L. N., Chung, K., and Kim, D. H. (2016). Plasmonic solar cells: from rational design to mechanism overview. *Chem. Rev.* 116, 14982–15034. doi:10.1021/acs.chemrev.6b00302
- Joshi, D. N., Krishnapriya, R., Korukunda, T. B., and Prasath, R. A. (2022). One-pot controlled microwave synthesis of Broadband-light absorbing irregular gold nanoparticles for solar cell application. *Sol. Energy* 240, 435–442. doi:10.1016/j.solener.2022.05.042
- Joshi, D. N., Sudhakar, S., Nair, R. V., and Prasath, R. A. (2017). Swift sol-gel synthesis of mesoporous anatase-rich TiO₂ aggregates via microwave and a lyophilization approach for improved light scattering in DSSCs. *J. Mater. Sci.* 52, 2308–2318. doi:10.1007/s10853-016-0523-2
- Jung, H. S., and Lee, J.-K. (2013). Dye sensitized solar cells for economically viable photovoltaic systems. *J. Phys. Chem. Lett.* 4, 1682–1693. doi:10.1021/jz400112n
- Kaur, N., Singh, D. P., and Mahajan, A. (2022). Plasmonic engineering of TiO₂ photoanodes for dye-sensitized solar cells: a review. *J. Electron Mater.* 51, 4188–4206. doi:10.1007/s11664-022-09707-3
- Krishnapriya, R., Praneetha, S., and Murugan, A. V. (2015). Energy-efficient, microwave-assisted hydro/solvothermal synthesis of hierarchical flowers and rice grain-like ZnO nanocrystals as photoanodes for high performance dye-sensitized solar cells. *CrystEngComm* 17, 8353–8367. doi:10.1039/c5ce01438g
- Li, X., Yang, W., Deng, J., and Lin, Y. (2023). Surface plasmon resonance effects of silver nanoparticles in graphene-based dye-sensitized solar cells. *Front. Mater.* 10, 1137771. doi:10.3389/fmats.2023.1137771
- Li, Z.-Q., Chen, W.-C., Guo, F.-L., Mo, L.-E., Hu, L.-H., and Dai, S.-Y. (2015). Mesoporous TiO₂ yolk-shell microspheres for dye-sensitized solar cells with a high efficiency exceeding 11%. *Sci. Rep.* 5, 14178. doi:10.1038/srep14178
- Lim, S. P., Pandikumar, A., Lim, H. N., Ramaraj, R., and Huang, N. M. (2015). Boosting photovoltaic performance of dye-sensitized solar cells using silver nanoparticle-decorated N,S-Co-Doped-TiO₂ photoanode. *Sci. Rep.* 5, 11922. doi:10.1038/srep11922
- Mandal, P., and Sharma, S. (2016). Progress in plasmonic solar cell efficiency improvement: a status review. *Renew. Sustain. Energy Rev.* 65, 537–552. doi:10.1016/j.rser.2016.07.031
- Mohammadian-Sarcheshmeh, H., Arazi, R., and Mazloum-Ardakani, M. (2020). Application of bifunctional photoanode materials in DSSCs: a review. *Renew. Sustain. Energy Rev.* 134, 110249. doi:10.1016/j.rser.2020.110249
- Moradi, A., Abrari, M., and Ahmadi, M. (2020). Efficiency enhancement in dye-sensitized solar cells through the decoration of electro-spun TiO₂ nanofibers with Ag nanoparticles. *J. Mater. Sci. Mater. Electron.* 31, 16759–16768. doi:10.1007/s10854-020-04231-8
- O'Regan, B., and Grätzel, M. (1991). A low-cost, high-efficiency solar cell based on dye-sensitized colloidal TiO₂ films. *Nature* 353, 737–740. doi:10.1038/353737a0
- Sharifi, N., Dabirian, A., Danaei, D., and Taghavinia, N. (2016). Aggregates of plasmonic nanoparticles for broadband light trapping in dye-sensitized solar cells. *J. Opt.* 18, 015902. doi:10.1088/2040-8978/18/1/015902

Funding

The author(s) declare that financial support was received for the research, authorship, and/or publication of this article. This work was supported by Science and Engineering Research Board, India, through a young scientist project under grant no. SR/FT/CS-164/2011 dated 04-12-2012. Author DNJ is thankful to the Ministry of New and Renewable Energy (MNRE), India, for the research fellowship.

Conflict of interest

The authors declare that the research was conducted in the absence of any commercial or financial relationships that could be construed as a potential conflict of interest.

Publisher's note

All claims expressed in this article are solely those of the authors and do not necessarily represent those of their affiliated organizations, or those of the publisher, the editors and the reviewers. Any product that may be evaluated in this article, or claim that may be made by its manufacturer, is not guaranteed or endorsed by the publisher.

- Tran, H. N., Nguyen, V. H., Nguyen, B. H., and Vu, D. L. (2016). Light trapping and plasmonic enhancement in silicon, dye-sensitized and titania solar cells. *Adv. Nat. Sci. Nanosci. Nanotechnol.* 7, 013001. doi:10.1088/2043-6262/7/1/013001
- Vemula, S. K., and Raavi, S. S. K. (2022). Ion-implantation in titania-based plasmonic photo-anodes: a review. *Adv. Mater Interfaces* 9, 2200085. doi:10.1002/admi.202200085
- Wang, H., Zheng, L., Liu, C., Liu, Y., Luan, C., Cheng, H., et al. (2011). Rapid microwave synthesis of porous TiO₂ spheres and their applications in dye-sensitized solar cells. *J. Phys. Chem. C* 115, 10419–10425. doi:10.1021/jp2011588
- Wang, Q., Butburee, T., Wu, X., Chen, H. J., Liu, G., and Wang, L. Z. (2013). Enhanced performance of dye-sensitized solar cells by doping Au nanoparticles into photoanodes: a size effect study. *J. Mater Chem. A Mater* 1, 13524–13531. doi:10.1039/c3ta12692g
- Yang, W.-G., Wan, F.-R., Chen, Q.-W., Li, J.-J., and Xu, D.-S. (2010). Controlling synthesis of well-crystallized mesoporous TiO₂ microspheres with ultrahigh surface area for high-performance dye-sensitized solar cells. *J. Mater Chem.* 20, 2870–2876. doi:10.1039/b923105f
- Zarick, H. F., Erwin, W. R., Boulesbaa, A., Hurd, O. K., Webb, J. A., Poretzky, A. A., et al. (2016). Improving light harvesting in dye-sensitized solar cells using hybrid bimetallic nanostructures. *ACS Photonics* 3, 385–394. doi:10.1021/acsp Photonics.5b00552